Location of Ryanodine and Dihydropyridine Receptors in Frog Myocardium

Pierre Tijskens,*† Gerhard Meissner,‡ and Clara Franzini-Armstrong*
*Department of Cell and Developmental Biology, University of Pennsylvania, Philadelphia, Pennsylvania 19104-6058; †Department of Anatomy and Human Physiology, University of Padova, Italy; and ‡Department of Biochemistry/Biophysics, University of North Carolina, Chapel Hill, North Carolina 27599-7260

ABSTRACT Frog myocardium depends almost entirely on calcium entry from extracellular spaces for its beat-to-beat activation. Atrial myocardium additionally shows internal calcium release under certain conditions, but internal release in the ventricle is absent or very low. We have examined the content and distribution of the sarcoplasmic reticulum (SR) calcium release channels (ryanodine receptors, RyRs) and the surface membrane calcium channels (dihydropyridine receptors, DHPRs) in myocardium from the two atria and the ventricle of the frog heart using binding of radioactive ryanodine, immunolabeling of RyR and DHPR, and thin section and freeze-fracture electron microscopy. In cells from both types of chambers, the SR forms peripheral couplings and in both chambers peripheral couplings colocalize with clusters of DHPRs. However, although a low level of high affinity binding of ryanodine is detectable and RyRs are present in peripheral couplings of the atrium, the ventricle shows essentially no ryanodine binding and RyRs are not detectable either by electron microscopy or immunolabeling. The results are consistent with the lack of internal calcium release in the ventricle, and raise questions regarding the significance of DHPR at peripheral couplings in the absence of RyR. Interestingly, the free SR membrane in both heart chambers shows a low but equal density of intramembrane particles representing the Ca^{2+} ATPase.

INTRODUCTION

The relative contributions of Ca^{2+} influx from extracellular spaces and Ca^{2+} release from internal stores (the sarcoplasmic reticulum, SR) to excitation–contraction (e–c) coupling of cardiac muscle cells vary in different regions of the heart and in hearts from different species (Bassingthwaighte and Reuter, 1974; Reuter, 1974; Lederer, et al., 1989; see Bers, 1991, for a review). In the ventricle of rat heart, the SR is quite abundant and block of the SR Ca^{2+} pump by thapsigargin, resulting in depletion of the SR Ca^{2+} stores, reduces twitch tension and Ca^{2+} transients by 80% (Inesi et al., 1998). At the other end of the spectrum, frog myocardium relies on extracellular Ca^{2+}, SR Ca^{2+} release is of small magnitude and its role in e–c coupling has been debated (Kavaler, 1974; Anderson et al., 1977; Niedergerke et al., 1976; Niedergerke and Page, 1981a,b; Morad and Cleemann, 1987; Tunstall and Chapman, 1994). Indeed, it is thought that SR Ca^{2+} in frog myocardium is called into play only under conditions of adrenergic and/or P_2 purinergic stimulation (Niedergerke and Page, 1981b).

The influx of extracellular Ca^{2+} in cardiac muscle takes place either through the dihydropyridine receptors (DHPRs), L-type voltage sensitive Ca^{2+} channels, located in exterior membranes (plasmalemma and T-tubules; see Ashley et al., 1991; Stern and Lakatta 1992; Cannell et al., 1995) or through other mechanisms such as Na^+/Ca^{2+} exchange. Ca^{2+} release from the SR membrane is either via the ryanodine receptors (RyRs; see Coronado et al., 1994; Meissner 1994; Franzini-Armstrong and Protasi, 1997; Sutko and Airey 1997, for reviews), or possibly via the IP3 receptor (Niedergerke and Page, 1981b).

In cardiac muscle, activation of RyR is dependent on Ca^{2+} entry through DHPRs, and this interaction takes place at junctions called peripheral couplings, and dyads, between specialized domains of the SR and either surface membrane or T-tubules, respectively. DHPRs and RyRs are clustered in close proximity with each other at dyads and peripheral couplings and these junctions are also called Ca^{2+} release units (CRUs) on the basis of their function. Activation of additional, extrajunctional RyR clusters located at some distance from DHPRs (Sommer et al., 1991) must occur via a less direct mechanism, probably mediated by the Ca^{2+} entering the cell and/or released at peripheral CRUs (Mackenzie et al., 2001; Trafford et al., 2002).

Caffeine and ryanodine, two pharmacological agents that specifically affect the open probability and permeability of RyRs (Pessah et al., 1987; Rousseau and Meissner, 1989; Coronado et al., 1994; Ogawa, 1994), have been used to probe for SR Ca^{2+} release in frog heart. Interestingly, the effects of caffeine and ryanodine are quite different in atrium and ventricle. In frog atrium, high concentrations of caffeine ($\geq$10 mM) increase the strength of the contractures initiated by either high-potassium or sodium-free solutions, whereas low concentrations ($\leq$10 mM) enhance the twitch response (Chapman and Miller, 1974; Chapman and Miller, 1972; Niedergerke and Page, 1981a). In ventricle, on the other hand, the effect of caffeine is either absent (Niedergerke and Page, 1981a) or very small (Chapman and Miller, 1974), and the latter may be attributable to a direct effect on the

Submitted June 17, 2002, and accepted for publication October 17, 2002.
Address reprint requests to Clara Franzini-Armstrong, B42 Anatomy-Chemistry Building, Dept. of Cell and Developmental Biology, University of Pennsylvania School of Medicine, Philadelphia, PA 19104-6058. Tel.: 215-898-3345; Fax: 215-572-2170; E-mail: armstroc@mail.med.upenn.edu.

0006-3495/03/02/1079/14 $2.00

myofibrils at the high concentrations of caffeine used (S. Page, personal communication; see also Wendt and Stephenson, 1983). In frog atrium ryanodine leads to a transient increase in twitch tension if applied in the presence of caffeine, but seems to have no effect in its absence (Tunstall and Chapman, 1994). No effect of ryanodine was reported for the ventricle, even though a large range of concentrations was used (Ciofalo, 1973). However, inasmuch as no caffeine was used in these experiments, the results are not comparable with those in the atrium.

Finally, adrenaline and ATP in conjunction with the action potential facilitate the release of Ca from the SR in frog heart, but the responses were more readily obtained in atrium than in ventricle. The concentration of ATP required to give a weak response in the ventricle is 10-fold larger than the concentration producing a stronger response in the atrium (Niedergerke and Page, 1981b).

All these results lead to the conclusion that, even though as most, if not all, the Ca^{2+} required for the activation of the twitch tension in frog heart cells is supplied by the inward Ca^{2+} current through the surface membrane (Tunstall and Chapman, 1994; Niedergerke et al., 1976), atrial and ventricular cells may also rely on Ca^{2+} release from the SR under special conditions and to a smaller extent than in mammalian and avian myocardium. In addition, the release may be due to different mechanisms in the two heart chambers (see above).

With this in mind, it is interesting to consider the structure of the SR in frog myocardium. Myocytes in both atrium and ventricle have small diameter and no T-tubules (Page, 1968). The cells basically contain few myofibrils and a network of relatively scarce, but well-organized SR. In both atrial and ventricular myocytes, flattened SR sacs have one surface closely associated with the surface membrane, forming peripheral couplings (Page and Niedergerke, 1972; Bossen and Sommer, 1984; Duvert and Verna, 1985), a type of CRU typical of cardiac muscle (Sommer and Johnson, 1980; Bossen and Sommer, 1984; Sommer et al., 1991). The rest of the SR is free and it is expected to contain the Ca^{2+} pump protein. The surface densities of SR are greater in atrium than in ventricle (0.441 ± 0.067 vs. 0.264 ± 0.034 $\mu m^2/\mu m^3$, respectively) whereas the surface density of junctional SR is the same in the two chambers (Bossen and Sommer, 1984).

None of the above structural data are sufficient to explain the functional differences in Ca^{2+} release in atrium and ventricle. We have examined the distribution of RyRs and DHPRs in the two chambers of the frog heart, using electron microscopy in combination with immunolabeling at the light microscope level and ryanodine binding. We find that RyRs are present in limited amounts in peripheral couplings of the atrium, but are virtually absent from the ventricle. Unexpectedly, however, the disposition of DHPRs in clusters related to the position of peripheral couplings is qualitatively similar in cells from the two chambers.

MATERIALS AND METHODS

[^{3}H]ryanodine binding

The ryanodine receptor contents of atria and ventricle were determined by isolating the 3-[(3-cholamidopropyl) dimethyl-ammonio]-1-propanesulfonate (CHAPS)-solubilized, [^{3}H]ryanodine-labeled 30S receptor complexes by sucrose density gradient centrifugation. The experiments were done in duplicate. Either combined atria from three hearts or a complete ventricle were homogenized in a glass/ground glass homogenizer in 1 ml 1 M NaCl, 20 mM Na Pipes, pH 7.4, 100 μM EGTA, 400 μM Ca^{2+}, 1.5% CHAPS, 5 mg/ml 95% phosphatidylcholine (Avanti Polar Lipids, Alabaster, AL), 5 mM AMP, 0.2 mM Pefabloc 20 μM leupeptin, and 1 mM dithiothreitol. Homogenates were labeled for 30 min at 24°C with 35 nM [^{3}H]ryanodine (NEM Life Science Products, Boston, MA) in the absence and presence of 10 μM unlabeled ryanodine (Calbiochem, San Diego, CA). To localize RyRs on the gradients, 30S ryanodine receptor complexes were isolated by sucrose density gradient centrifugation (Anderson et al., 1989). Matched experiments were carried out with canine cardiac SR vesicles and the results were consistent with published data (Anderson et al., 1989). Radioactivity of the sucrose gradient fractions was counted by liquid scintillation to obtain [^{3}H]ryanodine comigrating with 30S receptor complexes in gradient fractions.

Electron microscopy

Whole hearts from adult *Rana temporaria* were quickly removed, opened by a single longitudinal cut through atria and ventricle, pinned to Sylgard with the trabeculae in a slightly stretched position, rinsed in frog Ringer's solution (KCl 2.5 mM, NaCl 115 mM, $CaCl_2$ 1.8 mM, and $NaPO_4$ buffer 3 mM) for a few minutes, and fixed in 6% glutaraldehyde in 0.1-M cacodylate buffer, pH 7.4. For thin sectioning, trabeculae were gently teased out, postfixed in 2% OsO_4 in cacodylate buffer for 1 h, en bloc stained in saturated aqueous uranyl acetate over night, and embedded in Epon 812. Thin sections were stained in ~4% uranyl acetate in 50% ethanol and with ''Sato'' lead (Sato, 1968).

For freeze-fracture, atrial and ventricular trabeculae were teased from the glutaraldehyde-fixed hearts, infiltrated with 30% glycerol, frozen in liquid-nitrogen-cooled propane, fractured, shadowed with platinum at 45°, and replicated with carbon in a model 400 Balzers freeze-fracture apparatus (Balzer, Fürstentum, Liechtenstein).

Thin sections and replicas were examined at 60 kV in a Philips 410 electron microscope (Philips Electron Optics, Mahwah, NJ).

Immunolabeling

For cryosections, the heart was quickly removed and large portions of the heart, including most of either atrium or ventricle, were frozen in liquid-nitrogen-cooled propane. Cryostat sections, 5–10 μm, were cut at −20°C. The frozen sections were fixed in methanol at −20°C for 30 min and rehydrated in phosphate-buffered saline (PBS; NaCl 140 mM, KCl 2.7 mM, Na_2HPO_4 15 mM, KH_2PO_4 1.5 mM, pH 7.4). For whole mount immunolabeling, hearts were quickly removed, opened and pinned, rinsed in frog Ringer's solution for 20 min, fixed in 1% paraformaldehyde and 0.5% Triton in PBS for 20 min at room temperature, and washed in PBS for 15 min. Small groups of trabeculae were dissected free.

Sections and whole mounts were blocked with PBS containing 1% bovine serum albumin (BSA) and 10% goat serum at 4°C for 1 h, incubated with primary antibody at 4°C overnight, with Texas Red-labeled secondary antibody for 1 h at room temperature with three washes in PBS–BSA in between, and mounted in antibleaching solution (0.0025% para-phenylenediamine, 0.25% 1, 4 diazobicyclo 2, 2, 2 octane, and 5% n-propylgallate in glycerol). In three single-labeling experiments, atrial and ventricular tissues were processed in parallel. For double labeling, sections and/or whole mounts were simultaneously incubated with a mixture of two primary

antibodies and then with a mixture of Texas Red- and fluorescein-labeled secondary antibodies. Specimens were examined with a confocal Zeiss LSM 510 microscope (Carl Zeiss, Switzerland). All antibodies were diluted into the PBS–BSA solution.

The primary antibodies used were: 34C, a mouse monoclonal antibody generated against avian RyR (Airey et al., 1990), which recognizes all types of RyRs across species (Developmental Studies Hybridoma Bank, The University of Iowa); CI2, a polyclonal antibody which recognizes the GST-tagged fusion protein containing residues 785–930 of the rabbit α_{1C} subunit of the L-type Ca^{2+} channel (Gao et al., 2000; kindly provided by M.M. Hosey); and an anti-s-α-actinin rabbit polyclonal antibody (Ojima et al., 1999). The following IP3 antibodies were tried without success: Chemicon (Cat. #MAB3078), against type 1,2,3; a polyclonal antibody against the C-terminus of rat (Takei et al., 1992), kindly donated by P. DeCamilli; CT1, a polyclonal antibody raised against a C-terminus peptide of rat type 1 IP3R (Wojcikiewjcz et al., 1994); three monoclonals (T1NH, T2NH, and T3NH) against the amino terminal regions of rat types 1–3 IP3R (kindly donated by G.A. Mignery).

The secondary antibodies used were: Texas Red-conjugated goat anti-mouse IgG (from Molecular Probes, Cat. #T-862); Texas Red-conjugated goat anti-rabbit IgG (from Cappel, Cat. #55675 and from Jackson Immuno Research Laboratories, Cat. #111-075-144); fluorescein (FITC)-conjugated goat anti-rabbit IgG (H+L; from Jackson ImmunoResearch Laboratories, Cat. #111-095-045); and fluorescein (FITC)-conjugated goat anti-mouse IgG (H+L; from Jackson ImmunoResearch Laboratories, Cat. #111-095-146).

Measurements

All micrographs for the measurements were collected using a criterion of randomness. Specifically, either the first fiber or the first peripheral coupling to appear on the EM screen for each grid opening was photographed.

The width of the junctional gap between SR and surface membrane of peripheral couplings was determined by measuring the distance between the cytoplasmic edges of the two membranes in EM micrographs taken at a magnification of 24,400× and digitally scanned at high resolution (1200 dpi), using the ''ruler'' tool of Adobe Photoshop.

Sarcomere length (between the center of two *Z*-lines) and the center-to-center distances between the *Z*-lines and either peripheral couplings (in thin sections) or clusters of particles (in freeze-fracture) were measured with a ruler on micrographs printed at final magnifications of 20–34,000×.

The surface areas of particle clusters were measured using NIH Image, from micrographs of freeze-fracture replicas taken at the magnification of 33,900×.

RESULTS

Ryanodine binding assays

Sucrose gradient experiments and radioactive ryanodine binding assays indicate an average RyR content of 20–50 fmol for the duplicate experiments using three combined atria from three frogs and less than 3 fmol for duplicate data from a single ventricle. The latter value is below the detection limit. By comparison, the RyR content of mouse and rat hearts is ~25 times higher than in frog atrium, when expressed on a protein basis (G. Meissner, unpublished data). Considering that the atria together have considerably smaller muscle mass than the ventricle (by a factor of 4, as indicated by a rough measurements of wet weights), this indicates that the content of RyR of atrium myocardium, even though much lower than in mammalian myocardium, greatly exceeds that in ventricle. Indeed, RyR appears to be essentially absent from ventricle. The RyR content of the atrium, however, is also very low compared with that in mammalian myocardium.

Immunohistochemistry

Fig. 1 shows longitudinally oriented optical sections from confocal images of atrial and ventricular trabeculae labeled with antibodies for RyR, α-actinin, and DHPR, singly or in combination. In both chambers, myocytes are very narrow and elongated. In a thin (~1-μm thick) optical section, the cell surface is seen either as parallel lines separated by distances of 5–10 μm where the optical section cuts the cells in the middle, or as a wide strip where the section is tangent to the cell surface. Images from whole mounts and frozen sections did not differ in any significant detail.

Labeling for RyR in atria results in rows of RyR-positive foci. The foci are located either along parallel longitudinal lines separated by 5- to 10-μm distances (Fig. 1 *A*, *arrows*), or in short, transversely oriented rows of 2–4 elements (Fig. 1 *A*, *arrowheads*). In the direction parallel to the fiber long axis, the foci are arranged in a sarcomere-related periodicity, in which either single intense foci (Fig. 1 *A*, *arrows*), or doublets of foci (Fig. 1 *B*, *double arrows*) are located at distances of ~2 μm. Double immunolabeling, for RyR (*red*) and for α-actinin (*green*, labeling the *Z*-lines), demonstrates that RyR foci are in close proximity to the myofibrils' edges, and are either at the level of the *Z*-lines or on either side of them (Fig. 1 *C*).

CI2, a primary antibody against the α1-cardiac subunit of the DHPR, reveals foci of DHPRs at the periphery of atrial cells (Fig. 1 *D*). The labeling pattern is similar to that shown by RyR, although the images show more nonspecific background staining. The DHPR foci are located in longitudinal rows at the intersection of the cell surface with the optical section, and they show a sarcomere-related periodicity (Fig. 1 *D*, *arrowheads*). Where the section grazes the cell surface, DHPR positive spots are aligned in small transversely oriented rows located at ~2-μm intervals.

Double immunolabeling of frozen sections from atrial trabeculae with antibodies 34C and CI2 reveals that foci of the two proteins occupy closely related positions and that there is frequent but not complete colocalization (*yellow*) of RyR (*red*) and DHPR (*green*) foci (Fig. 1, *E* and *F*). The colocalization is not perfect, as either the green (RyR) or the red (DHPR) labels extend in many instances beyond the area of overlap between the two, and also some foci are labeled exclusively by either antibody. This indicates that groups of RyRs and DHPRs are located in close proximity to each other, but that both proteins are not always simultaneously present at the same site and over an equivalent area of membrane.

In ventricle, no RyR foci were detected even using the highest intensity gain in the confocal microscope (Fig. 2). The presence of RyR-antibody clusters in atrium and the

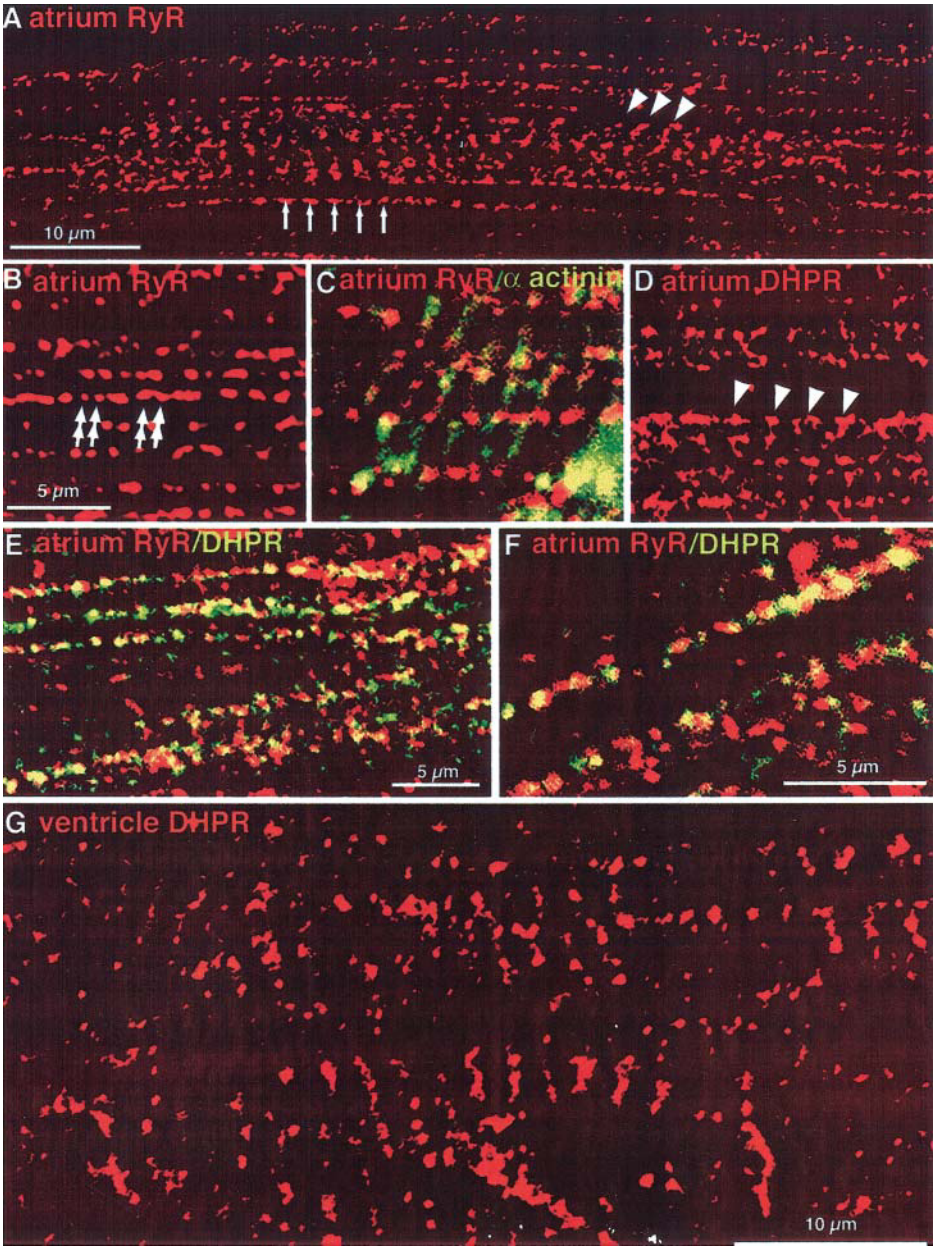

FIGURE 1 Whole mounts (*A*,*B*) and frozen sections (*C*–*G*) of atrial and ventricular myocardium labeled with antibodies against RyR, DHPR, and α-actinin, a *Z*-line protein. Longitudinal axes of fibers are approximately horizontal. In the atrium, RyR-positive foci (*A*–*C*) are aligned along parallel lines that delimit the borders of the narrow cells (from *left* to *right* in the image). The spacing between adjacent RyR spots in the longitudinal direction is equal to the sarcomere length (*A*, *arrows*). Either a single or a double set of RyR foci are located at each sarcomere (*arrows* and *double arrows*, *A* and *B*). Where the plane of the confocal image happens to be parallel to one of the wider sides of a cell, the RyR foci are aligned in an approximately transverse direction (*arrowheads*). Double labeling for RyR and α-actinin (*C*) shows that RyR foci are located at or close to the position of the *Z*-lines. DHPRs are located in foci with a disposition similar to that of RyR foci (*D*), and double labeling for the two proteins indicates a frequent but not obligatory overlap of the foci position (*E* and *F*, *yellow spots*). In the ventricle (*G*), DHPR antibody labeling gives a *Z*-line-related position similar to that in the atrium, but RyR antibody (See Fig. 2) gives no labeling.

virtual absence in ventricle were confirmed in three separate experiments using parallel immunolabeling of both whole mounts and frozen sections from the two chambers. Given the fact that the antibody used recognizes different RyR in a large variety of vertebrate muscles (Airey et al., 1990; Olivares et al., 1991), and given the positive labeling of the atrium RyR, it is unlikely that lack of labeling in the ventricle could be assigned to a failure of the antibody to bind to RyR rather than to an absence of the protein. Ryanodine binding experiments (see above) and thin sections electron microscopy (see below) fully confirm this assumption. Labeling of ventricular trabeculae with anti-DHPR antibodies, on the other hand, revealed clusters of DHPR in foci arranged along transverse lines at sarcomeric spacings (Fig. 1 *G*) which are similar to those in trabeculae from atrium.

Electron microscopy

Thin sections

In both atrium and ventricle of frog myocardium, the SR forms a network of elongated sacs and flat cisternae. The latter lie mostly in the space between the myofibrils and the surface membrane (Fig. 3), as previously described (Page and Niedergerke, 1972; Bossen and Sommer, 1984). Here we focus on the flat cisternae that are closely apposed to the

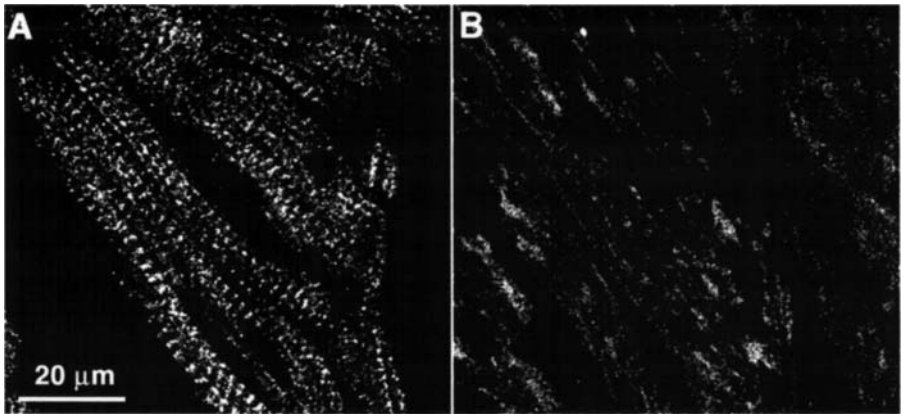

FIGURE 2 Comparison of labeling for RyR using 34C antibody in atrium (*A*) and ventricle (*B*). The image for the ventricle was recorded at a high gain in the confocal microscope, thus enhancing the finely granular nonspecific background which is also seen in the atrium between the positively labeled foci. The ventricle shows no periodically disposed brightly fluorescent foci. If taken with the same gain as Fig. 2 *A*, Fig. 2 *B* would be totally dark.

surface membrane. Most of the flat cisternae are in close apposition to the surface membrane from which they are separated by a small distance (Fig. 4, *A–E*). We consider all such cisternae as components of peripheral couplings, although close examination reveals that they are not all equal (see below). Cisternae that are not apposed to the surface and SR elements with smaller sectional profiles (not shown, but see Page and Niedergerke, 1972) are considered to be part of the free SR.

A closer look at the fine details of peripheral couplings shows variability in their structure and a significant difference between atrium and ventricle. In some peripheral couplings of the atrium the junctional gap between surface and SR membranes is occupied by several densities (feet) disposed at approximately equal intervals (Fig. 4, *A* and *B*, between *asterisks*; Fig. 4 *F* is a higher magnification of Fig. 4 *B*). The feet resemble those present in peripheral couplings and T–SR junctions of other cardiac muscle (Fawcett and McNutt, 1969; Sommer and Johnson, 1980; Bossen and Sommer, 1984; Sommer et al., 1991; Protasi et al., 1996; Sun et al., 1995). In the atrium, ~15% of peripheral couplings have such rows of feet (from a total of 203 couplings in atria from four frogs). An additional 15% of peripheral couplings have a few densities resembling feet, which are randomly distributed in the junctional gap (Fig. 4, *B* and *F*, *arrows*). These feet are less easy to identify, and some, particularly if present singly, are easily missed. The

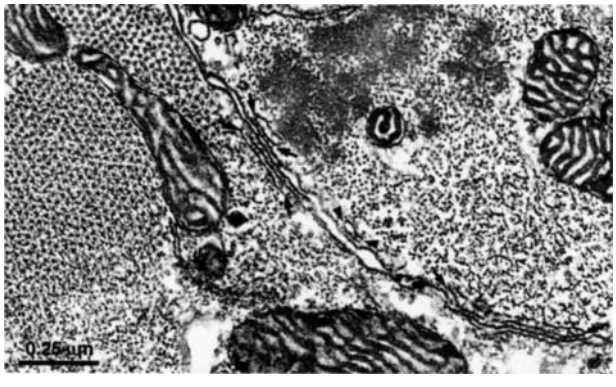

FIGURE 3 Cross section of two adjacent cells in the atrium. The narrow extracellular space runs obliquely in the image. The cell at the left is sectioned at the edges of the *A*-band and shows the transition between *A*- and *I*-bands (*A*, *I*). The cell on the right is sectioned approximately at the level of the *Z*-line and shows *Z*-line and *I*-band (*Z*, *I*). Three flat SR cisternae are closely apposed to the surface membrane (between *arrows*) and are part of peripheral couplings. A fourth SR vesicle (between *arrowheads*) is probably not a component of a peripheral coupling, but rather is part of the free SR, inasmuch as its lumen is empty (that is, it contains no calsequestrin).

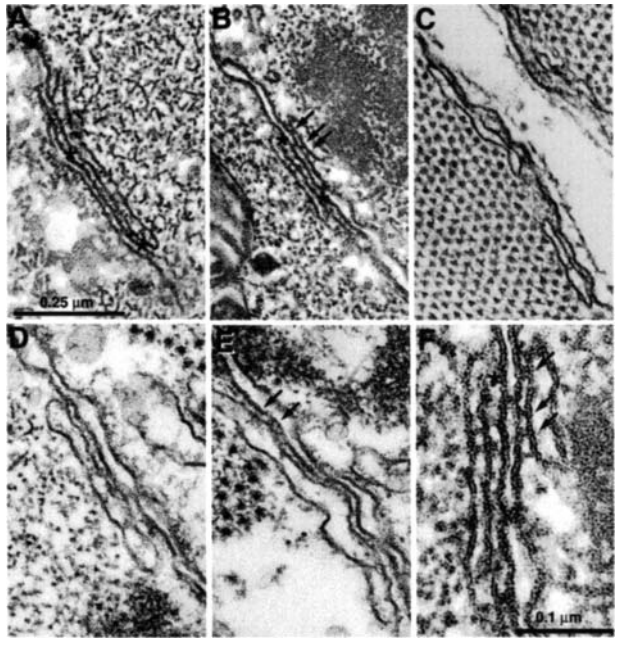

FIGURE 4 Details of peripheral couplings in the atrium (*A–C*, *F*) and the ventricle (*D*, *E*). In atrial cells, some peripheral couplings show a row of fairly evenly spaced feet in the junctional gap between the SR vesicle and the sarcolemma (*A*, *B*, *F* between *asterisks*). Other peripheral couplings have feet that do not completely fill the gap (*arrows* in *B* and *F*). Finally a fairly high proportion of the junctions show no feet (*C*). In ventricular cells none of the vesicles associated with the surface membrane show rows of feet (*D*), but a very small percentage show few single feet (*arrows*, *E*). *F* is a higher magnification of *B*.

majority of peripheral couplings (i.e., the remaining 70%) apparently lack feet (Fig. 4 *C*).

Peripheral couplings in ventricles lack periodically disposed feet (Fig. 4 *D*). A few (14% from a total of 175 junctions in four frogs) have occasional densities that may represent feet; however, these are not clearly delineated and are not periodically disposed (Fig. 4 *E*, *arrows*).

The size of the junctional gap separating SR and surface membranes is fairly constant in the peripheral couplings from the atrium that contain periodically disposed feet. In contrast, peripheral couplings that lack feet in atrium and ventricle have variable distances between SR and surface membrane, and sometimes the gap is large (Fig. 4 *C*).

The width of the junctional gap between the apposed SR and surface membranes was measured in peripheral couplings of atrial and ventricular myocytes from three frogs. For atrium, junctions were divided into three categories: those that contain a periodically disposed row of feet; those that have few, not clearly aligned feet; and those that lack feet. In all cases, the gap width was measured only along the portions of cisternal surfaces that are approximately parallel to the surface membrane. Segments of vesicle profiles that are clearly detached were not considered. The values for the gap width in the three types of junctions defined above are, respectively: (8.3 $\pm$ 1.5 nm, $n = 19$; 7.4 $\pm$ 1.2 nm, $n = 18$; 7.2 nm $\pm$ 1.6, $n = 86$; mean $\pm$ 1 SD, n = number of junctions). In ventricle junctions where few feet may be present, the gap is wider (9.0 $\pm$ 2.0 nm, $n = 19$) than in dyspedic junctions (7.4 $\pm$ 2.0, $n = 117$). The differences between junctions containing and lacking feet in atrium and ventricle are significant at *P*-levels of 0.0072 and 0.0015, respectively (Student's *t*-test).

Calsequestrin has a recognizable structural signature in the electron microscope. It appears as an electron-dense, fine-grained content in the lumen of junctional SR (Sommer, 1995; Jorgensen et al., 1985; Jewett et al., 1971; Jones et al., 1998). Calsequestrin is present in frog myocardium (MacLeod et al., 1991) and it is visible as granular density in the SR of atrial peripheral couplings with feet (Fig. 4, *A* and *B*). However, calsequestrin is less visible and/or absent in peripheral couplings that have no or few feet in both atrium and ventricle. It is also absent from the rest of the SR.

Freeze-fracture

In freeze-fracture replicas of both atrium and ventricle the cytoplasmic leaflet of the surface membrane shows clearly visible specialized membrane domains, containing clusters of large, tall particles (Fig. 5). Particles of variable and smaller sizes are mostly excluded from the special membrane domains. Exclusion of smaller particles is less complete in ventricle than in atrium leaflets. The large particles within the cluster are of a fairly uniform height and diameter, indicating a homogenous protein composition. The average particle diameters measured perpendicular to the direction of shadowing are 10.0 $\pm$ 1.6 nm for atrium and 9.4 $\pm$ 1.6 nm for the ventricle (mean $\pm$ 1 SD, from 100 particles each). The minor difference between the two chambers is attributable to slight variations in the thickness of the platinum shadow.

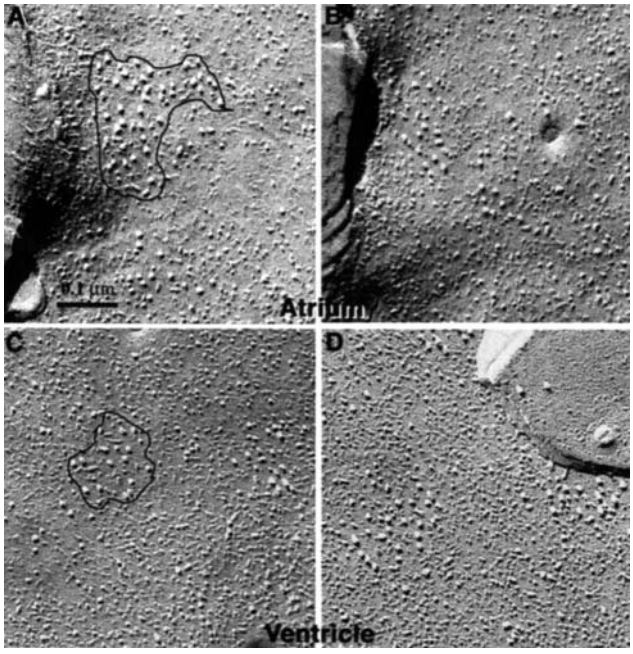

FIGURE 5 Images from freeze-fracture replicas of the plasmalemma in atrial (*A*, *B*) and ventricular (*C*, *D*) myocardial cells. Clusters of large particles are visible in the cytoplasmic leaflet. The size of the domains occupied by large particles and the total number of particles in each cluster vary, but in general both parameters are larger in atrium than in ventricle. Two characteristics of these clusters of particles resemble those of DHPR-containing membrane domains in avian myocardium: the particles are unusually tall and large in diameter, and smaller particles are mostly excluded, although the exclusion is not as stringent in the ventricle as it is in the atrium. The outlines in (*A*) and (*C*) indicate the approximate boundaries that were used to delimit the areas to be measured (see text for discussion of measurement accuracy).

The relationship between peripheral couplings and clusters of large membrane particles is illustrated by occasional images where the fracture plane jumps from the surface membrane into the adjacent SR. Fig. 6 *A* shows a portion of the surface membrane occupied by a cluster of large particles. On the left of this region, the fracture breaks into the cell and shows two SR tubules. The lower of the two tubules begins to widen (*arrowhead*) and comes to close proximity of the surface membrane immediately below the site occupied by large particles. In Fig. 6 *B*, the fracture shows the luminal leaflet of the junctional SR occupied by the intramembrane regions of the foot protein (*arrows*; compare with Fig. 2 of Felder and Franzini-Armstrong, 2002). The area of surface membrane immediately above the junctional SR shows the edge of one of the large particle clusters, with a smooth membrane and few large particles. The rest of the particle cluster is broken off.

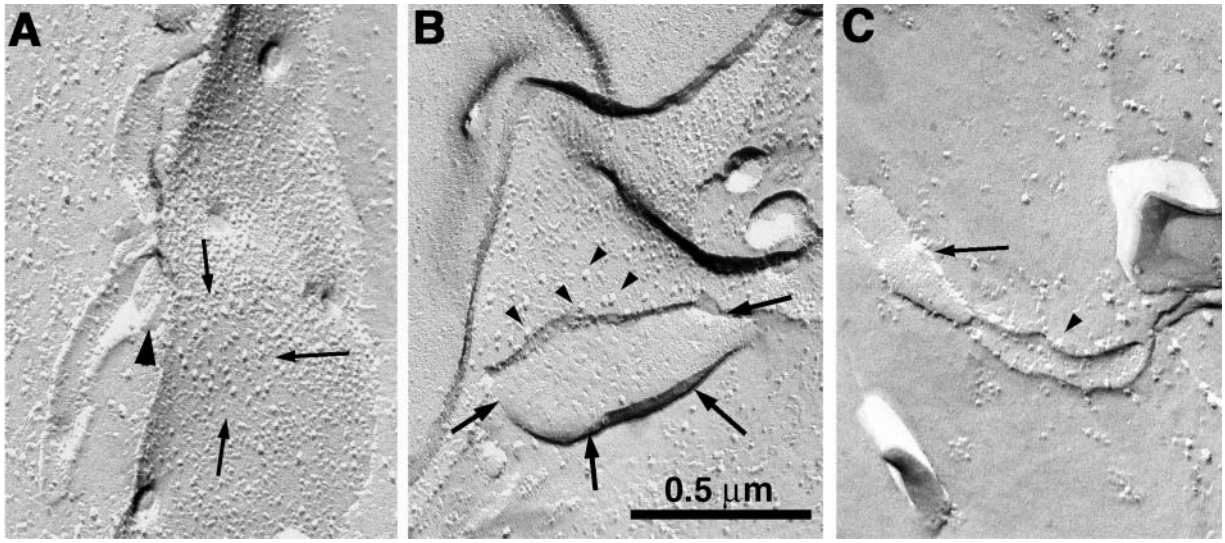

FIGURE 6 Freeze-fracture of atrial (*A* and *B*) and ventricular (*C*) myocytes showing SR membranes. (*A*) Cytoplasmic leaflets of two elongated, free SR vesicles. The relatively scarce small particles are fractures through the SR ATPase. The SR approaches the surface membrane at the arrowhead and presumably continues right under the membrane. The adjacent surface membrane contains a patch of large intramembranous particles (between *arrows*). (*B*) The luminal leaflet of the SR between arrows shows small pits surrounded by shallow bumps characteristic of the fractured intramembrane region of RyRs in the SR membrane (Block et al., 1988; Felder and Franzini-Armstrong, 2002). The transition from generic to large particle patch is seen in the adjacent surface membrane, where some large particles are present (*arrowheads*) and smaller particles are mostly absent. (*C*) Luminal (*arrow*) and cytoplasmic (*arrowhead*) leaflets of free SR in the ventricle. The cytoplasmic leaflet has a small number of intramembranous particles.

The position of peripheral couplings and particle clusters relative to the bands of myofibrils

Electron micrographs of longitudinal sections and freeze-fractures from atrial and ventricular trabeculae, such as shown in Figs. 7 and 8, were used to determine the position of peripheral couplings and clusters of particles relative to the bands of the myofibrils. This allowed us to directly compare the disposition of the particle clusters with that of peripheral couplings in a large sample. In thin sections of both atrium and ventricle (Fig. 7) the position of peripheral couplings (indicated by a *semicircle*) is either opposite the *Z*-line, or, more frequently, on either side of it (as previously described by Page and Niedergerke, 1972). Few peripheral couplings in each muscle are present in proximity to the *A*-band. In freeze-fracture images of the surface membrane (Fig. 8), large particle clusters are mostly located within a strip of membrane that extends up to 0.5 μm on either side of small linear depressions of the membrane that correspond to the *Z*-line positions of the underlying myofibrils.

The distance between the center of the *Z*-line and the center of peripheral couplings was measured in randomly collected images from thin sections similar to those shown in Fig. 7. To compensate for variations in sarcomere length at the moment of fixation, the data are presented in Fig. 9 (*dotted bars*) as the frequency distribution of the ratio between the *Z*-peripheral coupling distance and the sarcomere length. This ratio is 0 for peripheral coupling cisternae centered on the *Z*-line and 0.5 for those centered on the *M*-line. In both chambers the highest frequency is in the proximity of the *Z*-line.

The distances between the centers of *Z*-lines and the centers of particle clusters, was measured from a collection of random micrographs analogous to those shown in Fig. 8. The ratio between the *Z*-particle cluster distance and the sarcomere length is shown in Fig. 9 (*solid bars*). It is clear that the distribution of peripheral couplings and clusters of large particle clusters over the fiber surface is the same for atrium and ventricle and for the two types of structures.

Overall density of large clustered particles

To determine the total density of DHPRs per cell surface area, we determined the mean density of DHPR clusters per surface area, and counted the number of particles per cluster. The surface density of DHPR clusters relative to the cell surface area is approximately three times higher in atrial than in ventricular cells. The clusters were counted on montages of electron micrographs covering extended areas of cell surface (see Fig. 8) and the results indicate densities of 0.7 ± 0.2 clusters/μm^2 of cell surface $n = 5$ cells and 0.2 ± 0.1 clusters/μm^2, $n = 8$ respectively for atrium and ventricle. Atrial clusters contain 37 ± 23 particles (mean $\pm$ 1 SD, $n = 67$ clusters), vs. 20 ± 14 ($n = 47$) or ventricular clusters. The accuracy of particle counts is affected by the fact that the boundaries of the cluster are not always very clear, and thus it is sometimes difficult to decide whether some of the more

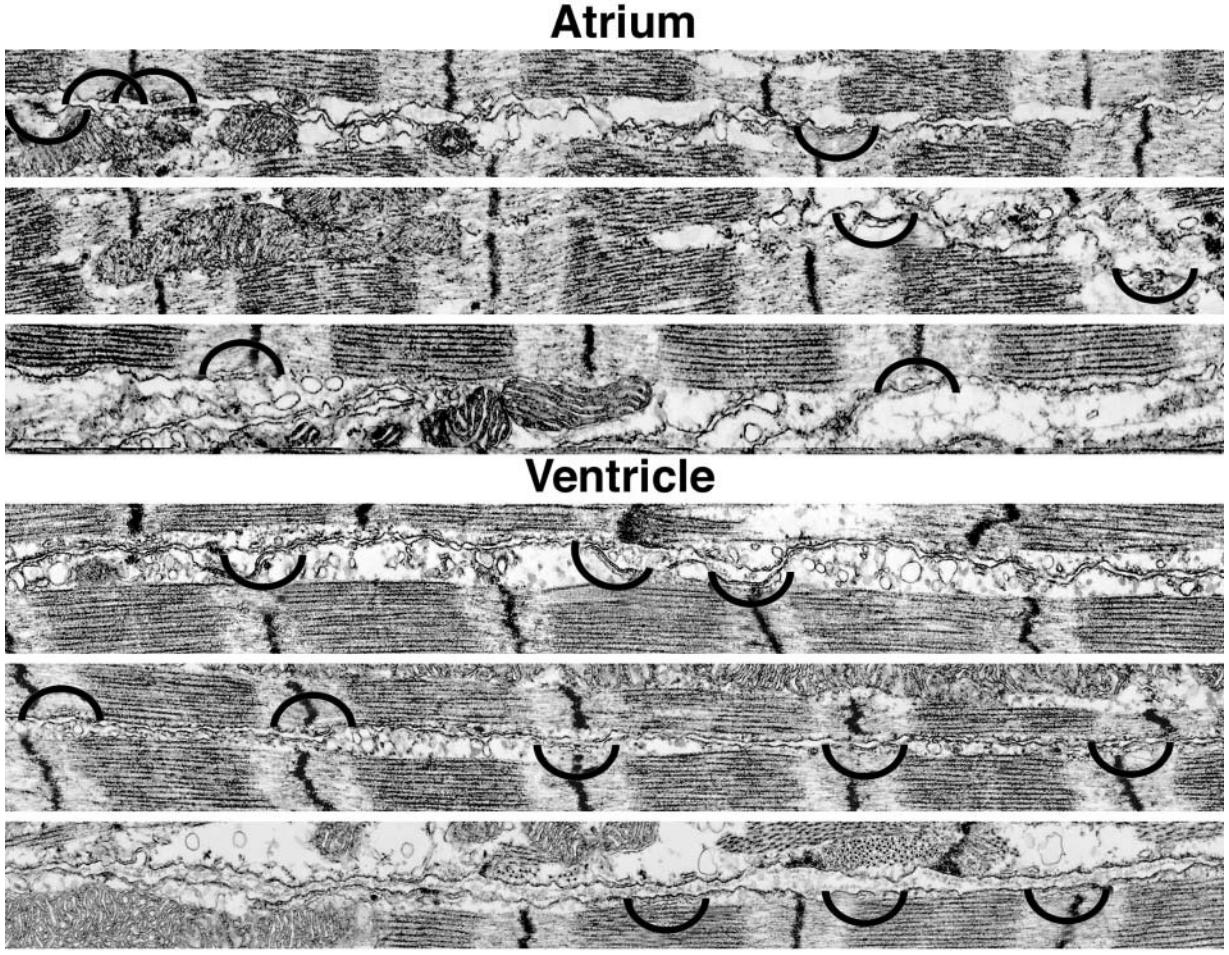

FIGURE 7 Montage of images from longitudinal sections of atrial and ventricular trabeculae. Each image shows narrow strips at the fibers' edges. The sites of peripheral couplings are not clearly visible at this magnification, but are indicated by semicircles. Most of peripheral couplings are located at or near the *Z*-lines (*Z*) of the nearest myofibrils. A few are located opposite the central region of the *A*-band.

peripheral particles belong to the cluster or not. This affects the data for ventricle more strongly than those for atrium, because in the latter the clusters are larger. An idea of the error involved can be derived by considering that if five particles at the periphery of each patch have uncertain assignment, the maximum error is 13% in atrium and 23% in the ventricle. The average error will be no more than one-half of those values.

The density of DHPRs was estimated by measuring the surface area of each DHPR cluster and obtaining the ratio of particle number/surface area independently for each cluster. The surface area measurements are affected by an uncertainty due to the precise position of the boundary line used to measure the area. Repeated measurements on the patch shown in Fig. 5 *A*, made by drawing boundary lines that followed the outline of the patch either very closely or more peripherally gave a variations of ~8% in the areas measured. The total area is also affected by the uncertainty in assigning some peripheral particles to the patch (see above), but the particle density is not affected by this source of variation because if particles are excluded from the measurements, so is the area in which they are located. The surface area of the clusters is larger in the atrium than in the ventricle ($25.7 \pm 17.7 \times 10^{-3}$ μm^2, $n = 67$ clusters; $11.6 \pm 10.5 \times 10^{-3}$ μm^2, $n = 47$ respectively), but the density of particles within the cluster is not very different between the two chambers: $1{,}555 \pm 392$ particles/μm^2 for the atrium, and $1{,}876 \pm 426$ particles/μm^2 for the ventricle.

From the above data we calculate that the average density of clustered large particles, in relation to the total cell surface area, is 28/μm^2 for atrium and 4/μm^2 for ventricle.

Correlations between EM and immunolabeling data

Comparison of images from single- and double-immunolabeled optical sections and from the two EM techniques allows a better understanding of the distribution of RyR and

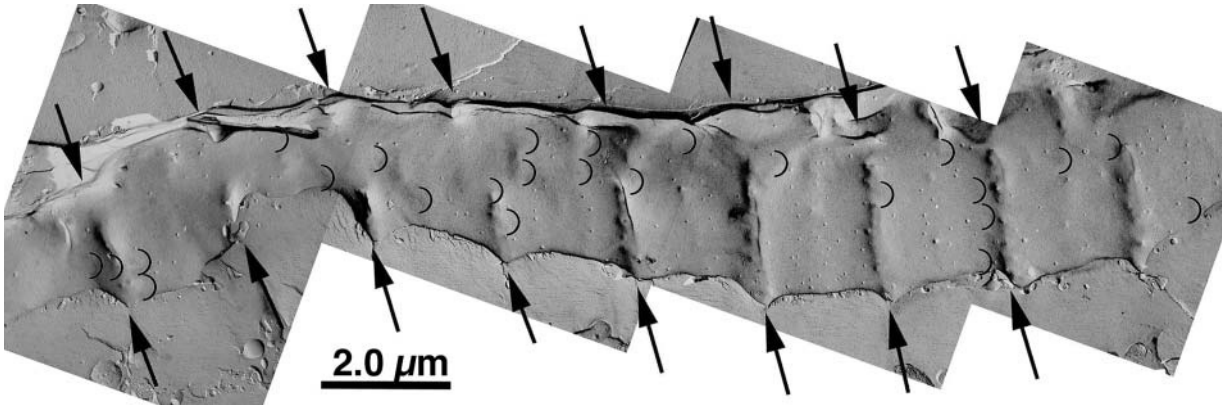

FIGURE 8 Montage of low magnification images from a freeze-fracture replica of the plasmalemma in an atrial cell. Arrows point to slight furrows that indicate the *Z*-line position of the underlying myofibrils. The positions of particle clusters (visible at higher magnification) are indicated.

DHPRs. First, the overall distribution of RyR- and DHPR-positive foci in the optical images is quite similar, particularly in showing foci that are aligned along parallel longitudinal lines. In the case of DHPRs, which are surface membrane channels, this must occur where the optical section bisects the cell surface. In the case of the RyR foci, the longitudinal lines might indicate a location of RyR positive spots either at the cell surface or between the two to three myofibrils that are present in each cell. The latter situation, however, is excluded by the observation that feet-bearing SR cisternae are observed only at the cell surface and that the positions of RyR- and DHPR-positive foci coincide.

When comparing immunolabeling images (Fig. 1) and thin section electron micrographs (Fig. 7) of atrial cells it might seem at first sight that the frequency of RyR-positive foci seen at the light microscope level far exceeds that of feet-bearing SR cisternae, particularly considering that only 30% of peripheral couplings appear to have feet. The effect, however, is simply due to differences in section thickness, which is at least 10-fold higher in the optical images (1–2 μm), than in the thin sections ($\sim$100 nm). The effect of section thickness is graphically illustrated in Fig. 10. The figure was obtained using three micrographs in a random series from thin sections of atrial cells similar to those illustrated in Fig. 7, as follows. The position of each peripheral coupling was marked by a large dot and the locations of *Z*-lines were noted. Twelve profiles of the fiber edges were copied and superimposed, using the *Z*-lines for alignment, to mimic the amount of material that would be included in a $\sim$1.2-μm thick section. Sarcomere lengths were adjusted to superimpose the *Z*-lines. The actual images were then eliminated, leaving only the positions of the *Z*-lines and of peripheral couplings, which are illustrated in Fig. 10. Note that at the level of each *Z*-line there are several couplings, so that even if only 30% of the couplings present have feet, each *Z*-line would have at least one RyR-positive spot in its proximity, as seen in the confocal images. Also, some spots are centered on the *Z*-lines, whereas others lie on either side of them, as also seen in the confocal images.

The relative frequencies of peripheral couplings and DHPR clusters in atrial cells were roughly estimated as follows. A small number of micrographs were ''randomly'' selected by accepting the first appropriate images that presented themselves on perusing our collection of micrographs. The basis for accepting images were: good fixation and section orientation for thin sections and a surface that covered several sarcomeres with good visibility of *Z*-lines location in the freeze-fractures. The number of peripheral couplings and the number of *Z*-lines were counted along 39 fiber edges each containing two to ten *Z*-line profiles in micrographs from thin sections similar to those shown in Fig. 7. The outlines of DHPR clusters and the *Z*-line positions were marked on prints from freeze-fracture images of the type used for constructing Fig. 8. A thin slit of 100-nm width and several sarcomere length (in real dimensions) was cut in a sheet of paper, superimposed on the image in a longitudinal orientation, and moved at variable intervals across the image. The number of clusters and *Z*-line positions visible through the slit was noted in 39 profiles mostly covering four *Z*-lines. The ratio of peripheral couplings to *Z*-line ends in thin sections is 1:2.6, and the ratio of particle clusters to *Z*-line sites on freeze-fracture images is 1:2.8. This indicates that clusters of DHPRs are associated with all peripheral couplings in the atrium, regardless of the presence of RyRs, and is in agreement with the observations in the ventricle, where particle clusters are apparently associated with peripheral couplings even though the latter do not contain RyRs.

The values from the above analysis indicate that there should be a predominance of DHPR- versus RyR-containing membrane regions in the atrium. The double immunolabel-

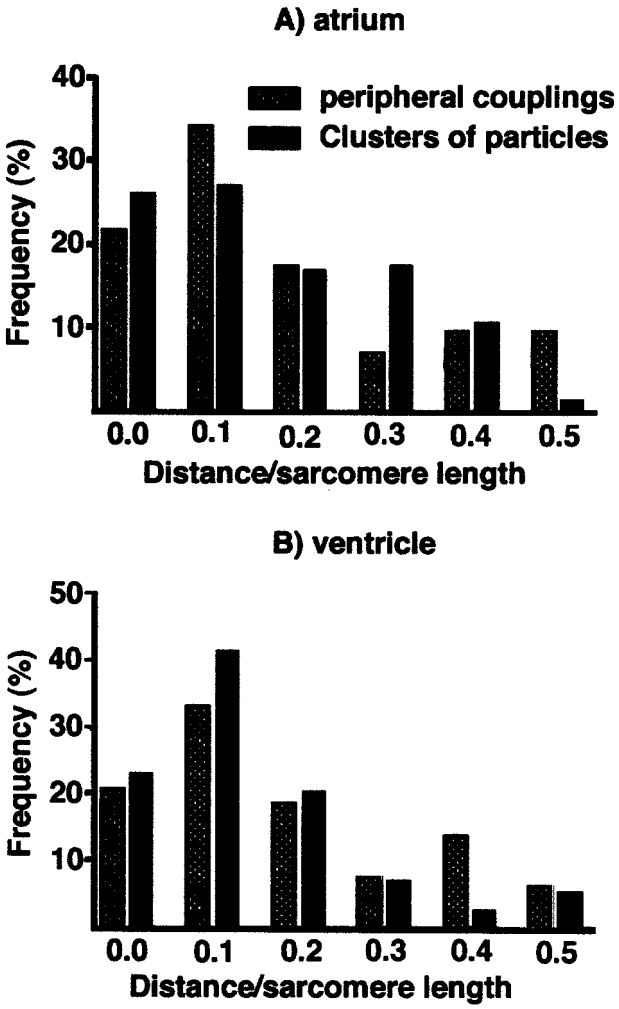

FIGURE 9 Frequency distribution of the ratios between the *Z*-line-to-peripheral coupling distance and the sarcomere length measured from thin sections (*dotted bars*), and of the ratios between the *Z*-line-to-particle cluster distance and the sarcomere length measured from freeze-fracture replicas (*solid bars*). A ratio of 0.5 indicates a position opposite the center of the *A*-band. The majority of peripheral couplings in both atrium (*A*) and ventricle (*B*) are located at or in proximity to the *Z*-line; fewer are opposite the *A*-band of the neighboring myofibrils.

ing image shown in Fig. 1 was selected from an area exhibiting a maximum amount of overlap between RyR and DHPR foci, demonstrating colocalization. Other areas of the confocal images from the double labeling, however, show a predominance of labeling for DHPRs over that for RyR.

SR membrane particles

The membrane of the free SR is occupied by randomly disposed particles of variable but mostly small size on the cytoplasmic leaflet (Fig. 6, *A* and *C*). The particles resemble in size and disposition those representing the calcium pump ATPase (Franzini-Armstrong and Ferguson, 1985). The density of particles was counted in fractured SR profiles from atrium and ventricle, giving average values of 1256 ± 662/μm^2 (mean ± SD, $n = 39$ vesicles) in atrium and 1200 ± 429/μm^2 ($n = 32$) in ventricle.

DISCUSSION

Our observations provide a structural foundation for the unusual properties of e–c coupling in frog myocardium. The basis for this work is our ability to detect and quantitate the content of ryanodine and dihydropyridine receptors. RyRs were identified by their characteristic structure in electron micrographs, with the confirmation by immunolabeling and ryanodine binding studies. Three sets of data are internally consistent. As in the case of skeletal and other cardiac muscles (Jorgensen et al., 1993; Junker et al., 1994; Takekura et al., 1994; Sun et al., 1995; Protasi et al., 1996), we find that the presence and location of feet in thin sections of atrium coincides with the presence and location of RyR foci detected by confocal microscopy using immunolabeling. The relatively low level of ryanodine binding to the atrium, as compared to the ~25 times higher binding levels to mouse and rat hearts, corresponds well with the scarcity of feet seen in thin sections. In ventricle, the absence of RyR foci and the undetectable level of ryanodine binding fit well with the EM observations indicating lack of feet.

DHPRs were identified by comparing electron microscopy and immunolabeling data as previously published (See Franzini-Armstrong and Protasi, 1997, for a review). Freeze-fracture indicates the presence and location of large intramembrane particles within well delimited clusters that closely correspond to the location of DHPR foci detected by immunolabeling in both atrium and ventricle. The par-

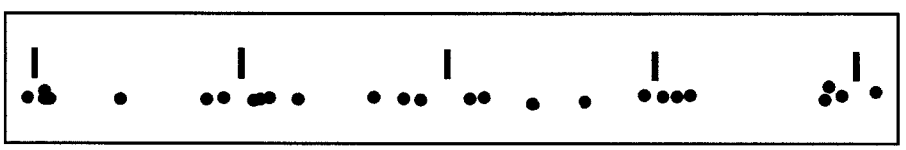

FIGURE 10 Predicted position and number of peripheral couplings visible in a optical section of ~1.2-μm thickness at the periphery of an atrial cell. The figure was constructed from thin section electron microscopy images as described in the text. The positions of *Z*-lines are indicated by bars. Each dot represents one peripheral coupling.

ticles have the same size (10.0 nm for atrium and 9.4 nm for the ventricle) as those identified with DHPRs in cells of skeletal muscle origin (9.9 nm, Protasi et al., 1998) and in chick cardiac muscle (8.5 nm, Sun et al., 1995), allowing us to extend the identification to the frog myocardium. From the correspondence in the positions of DHPR clusters and of peripheral couplings, we deduce that DHPRs occupy domains of the surface membrane that are associated with underlying SR cisternae.

The most striking result from these studies is the observation that ryanodine receptors are virtually absent in the ventricle of the frog myocardium. The finding is not unexpected in view of the physiological evidence for a lack of a calcium-releasing action of caffeine on the ventricle (see Introduction), but it does put the frog ventricle in a very special category. To our knowledge, all muscle cells and a large variety of nonmuscle cells contain ryanodine receptors, and release from intracellular stores via these channels contributes significantly to calcium transients. Frog ventricle seems to rely exclusively on calcium entry through the surface membrane. This is not inappropriate in cells that have very small diameters. However, a variety of muscle fibers that have very large inward Ca^{2+} currents, numerous T-tubules and/or small cell diameters, such as scorpion muscle (Gilly and Scheuer, 1984), body muscle of amphioxus (Benterbusch and Melzer, 1992; Benterbusch et al., 1992), fast adductor muscles of the scallop (Nunzi and Franzini-Armstrong, 1981), smooth muscles of vertebrates (Devine et al., 1972), atrial myocardium in many species, and all avian myocardium (Junker et al., 1994; Carl et al., 1995), do have the machinery for internal calcium release via RyRs. The frog ventricular myocytes remains for the time being the only known muscle to lack this internal calcium release mechanism.

The frog atrium seems to conform more closely than the ventricle to the standard calcium release unit composition of mammalian and avian cardiac myocytes, inasmuch as at least a portion of peripheral couplings in frog atrium show the usual close spatial association of DHPR and RyRs. The sparse presence of couplings is in accord with observations that release of Ca^{2+} from the SR in the atrium plays a minor role in steady-state e–c coupling and may come into play only in the case of α-adrenergic and/or P_2-purinergic stimulation (Niedergerke and Page, 1981b). The underlying structural cause for this reluctance to activate the internal release may lie in the relative scarcity of RyRs in the peripheral couplings of this muscle. Thus extra stimulatory mechanisms may be necessary to obtain a detectable release of Ca^{2+} from the SR in frog atrium.

Beside RyR, another Ca^{2+} release channel, the IP3 receptor, may contribute to internal Ca^{2+} release in frog heart, being activated as a result of the effect of external ATP (Niedergerke and Page, 1981b). IP3 receptors (Berridge, 1993) are known to be present in some cardiac muscles (Kijima and Fleischer, 1992; Kijima et al., 1993; Lipp et al., 2000). However, we were not able to detect IP3 receptors in the frog myocardium despite using a variety of available antibodies, perhaps because these antibodies did not cross-react with the frog isoform. If IP3 receptors were located in the cisternae of peripheral couplings, their presence, perhaps together with RyRs, would explain why the average junctional gap of frog peripheral couplings (between 7 and 9 nm) is always smaller than the gap in peripheral couplings of other cardiac and skeletal muscles that contain well-defined arrays of feet ($\sim$12 nm in mouse skeletal muscle, Takekura et al., 1995; $\sim$11 nm in chick cardiac muscle, Protasi et al., 1996).

Despite the difference in content of ryanodine receptors, SR of frog atrial and ventricular myocytes have essentially the same density of Ca^{2+} ATPase in the SR membrane, as shown by the similar density of intramembranous particles in the free SR. The free SR is the site where the Ca^{2+} ATPase is located and the density of membrane particles in this membrane is directly related to the density of Ca^{2+} ATPase (Franzini-Armstrong and Ferguson, 1985). The maximum ATPase/volume density in frog myocardium can be calculated using the data of Bossen and Sommer (1984) for the SR surface/volume ratio and assuming that all intramembrane particles in the freeze-fractured free SR membrane represent clusters of two to four (average, three) ATPase molecules (see Franzini-Armstrong and Ferguson, 1985). The ATPase density is at the most $1659/\mu m^3$ in atrial and $945/\mu m^3$ in the ventricular cells. These values are 10 times lower than the content of SR ATPase in slow- and fast-twitch skeletal muscle fibers (Ferguson and Franzini-Armstrong, 1988) and 200-fold lower than the ATPase content in a super-fast skeletal muscle (Appelt et al., 1991). Thus the frog cardiac SR has a limited role in relaxation, consistent with its limited role during excitation–contraction coupling. The calcium ions that are taken up by the ventricular SR may be necessary for maintaining the housekeeping roles of the membrane system (chaperoning proteins, etc.) and may exit the SR either via a very limited number of RyRs, or via IP3 receptors.

DHPRs in frog myocardium are clustered at sites of peripheral couplings, even though the latter contain no feet in the ventricle and often lack feet in the atrium. This is not entirely surprising, in view of the fact that DHPRs are appropriately targeted to calcium release units in ''dyspedic'' skeletal muscles resulting from null mutations of RyR1. Thus targeting of DHPRs to junctional sites is independent of the presence of RyR (Protasi et al., 1998; Takekura and Franzini-Armstrong, 1999; Felder et al., 2002). In skeletal muscle the signal to target DHPRs in the triad is located in the C-terminus of the DHPR α_{1s} subunit (Flucher et al., 2000). Perhaps the same targeting signal is used by the DHPR α_{1c} subunit of frog cardiac muscle, leading to DHPR clusters. Location of clusters near *Z*-lines is fascinating because it is at the same location where DHPRs are found in cardiac muscle having RyRs. During differentiation of avian

cardiac muscle and mammalian skeletal muscle, docking of SR to surface membrane/T-tubules precedes delivery and/or detention of DHPRs and RyRs at CRUs, indicating that SR docking guides the location of the junctional sites (Protasi et al., 1996; Takekura et al., 2001). However, this leaves the functional meaning of DHPR clustering at junctional domains open to question. Why should DHPRs be clustered at sites of peripheral coupling if, particularly in the case of the ventricle, they do not interact either functionally or structurally with RyRs?

The density of large particles present in the junctional domains of the plasmalemma, when referred to the total cell surface area, is larger in atrial than in ventricular cells (28 vs. $5/\mu m^2$). This is in strong contrast to the measured values of L-type Ca^{2+} current densities, which are higher in ventricle than in atrium, 3.4 ± 2.5 $\mu A/cm^2$ vs. 1.6 ± 2.5 $\mu A/cm^2$ (Hartzell and Simmons, 1987). There are two possible explanations for this apparent discrepancy. One is simply that atrium and ventricle differ in the extent of DHPR clustering, so that in ventricular cells the majority of Ca^{2+} channels are dispersed over the cell surface and a small proportion are in the junctional clusters, whereas in the atrium the majority of DHPRs are clustered. Our approach detects only the clustered channels and cannot identify the channels that are dispersed. A second, more interesting possibility is that the open probability of calcium channels under basal conditions is not the same in atrium and ventricle. Bean et al. (1984) showed that β-adrenergic stimulation increases the average number of functional Ca channels per cell in frog ventricle. Perhaps the atrium has an excess of channels which are less active.

We thank Dr. Sally Page for extensive reviewing of the manuscript and numerous stimulating suggestions, and Dr. Donald Bers for a discussion of DHPR content in cardiac muscle.

This research was supported by grant RO1 HL 48093 from the National Institutes of Health.

REFERENCES

Airey, J. A., C. F. Beck, K. Murakami, S. J. Tanksley, T. J. Deerinck, M. Ellisman, and J. Sutko. 1990. Identification and localization of two triad junction foot protein isoforms in mature avian fast twitch skeletal muscle. *J. Biol. Chem.* 265:14187–14194.

Anderson, K., F. A. Lai, Q. Y. Liu, E. Rousseau, H. P. Erickson, and G. Meissner. 1989. Structural and functional characterization of the purified cardiac ryanodine receptor–Ca^{2+} release channel complex. *J. Biol. Chem.* 264:1329–1335.

Anderson, T. W., C. Hirsch, and F. Kavaler. 1977. Mechanism of activation of contraction in frog ventricular muscle. *Circ. Res.* 41:472–480.

Appelt, D., V. Shen, and C. Franzini-Armstrong. 1991. Quantitation of Ca ATPase, feet and mitochondria in super-fast muscle fibres from the toadfish, *Opsanus tau. J. Muscle Res. Cell Motil.* 12:543–552.

Ashley, C. C., I. P. Mulligan, and T. J. Lea. 1991. Ca^{2+} and activation mechanisms in skeletal muscle. *Quart. Rev. Biophys.* 24:1–73.

Bassingthwaighte, J. B., and H. Reuter. 1974. Calcium movements and excitation-contraction coupling in cardiac cells. *In* Electrical Phenomena of the Heart. W.C. De Mello, editor. Academic Press, New York. 353–395.

Bean, B. P., M. C. Nowycky, and R. W. Tsien. 1984. β-adrenergic modulation of calcium channels in frog ventricular heart cells. *Nature.* 307:371–375.

Benterbusch, R., R. Herber, W. Melzer, and R. Thieleczek. 1992. Excitation-contraction coupling in a pre-vertebrate twitch muscle: the myotomes of *Branchiostoma lanceolatum*. *J. Membr. Biol.* 129: 237–252.

Benterbusch, R., and W. Melzer. 1992. Ca^{2+} current in myotome cells of the lancelet (*Branchiostoma lanceolatum*). *J. Physiol.* 450:437–453.

Berridge, M. 1993. Inositol trisphosphate and calcium signaling. *Nature.* 361:315–325.

Bers, D. M. 1991. Ca regulation in cardiac muscle. *Med. Sci. Sports Exerc.* 23:1157–1162.

Block, B., A. Leung, K. P. Campbell, and C. Franzini-Armstrong. 1988. Structural evidence for direct interaction between the molecular components of the transverse tubules/sarcoplasmic reticulum junction in skeletal muscle. *J. Cell Biol.* 107:2587–2600.

Bossen, E. H., and J. R. Sommer. 1984. Comparative stereology of the lizard and frog myocardium. *Tissue Cell.* 16:173–178.

Cannell, M. B., H. Cheng, and R. A. Waugh. 1995. The control of calcium release in heart muscle. *Science.* 268:1045–1049.

Carl, S. L., K. Felix, A. H. Caswell, N. R. Brandt, W. J. Ball, Jr., P. L. Vaghy, G. Meissner, and D. G. Ferguson. 1995. Immunolocalization of sarcolemmal dihydropyridine receptor and sarcoplasmic reticular triadin and ryanodine receptor in rabbit ventricle and atrium. *J. Cell Biol.* 129:672–682.

Chapman, R. A., and D. J. Miller. 1972. Caffeine contractures induced in frog auricular trabeculae in the absence of external calcium. *J. Physiol.* 225:52P–54P.

Chapman, R. A., and D. J. Miller. 1974. The effects of caffeine on the contraction of the frog heart. *J. Physiol.* 242:589–613.

Ciofalo, F. R. 1973. Relationship between ^{3}H-ryanodine uptake and myocardial contractility. *Am. J. Physiol.* 225:324–327.

Coronado, R. J., M. Morrissette, M. Sukhareva, and D. M. Vaughan. 1994. Structure and function of ryanodine receptors. *Am. J. Physiol.* 266: 1485–1491.

Devine, C. E., A. V. Somlyo, and A. P. Somlyo. 1972. Sarcoplasmic reticulum and excitation-contraction coupling in mammalian smooth muscle. *J. Cell Biol.* 52:690–718.

Duvert, M., and A. Verna. 1985. Ultrastructure and architecture of the sarcoplasmic reticulum in frog sino-atrial fibers: a comparative study with various preparatory procedures. *J. Mol. Cell. Cardiol.* 17:43–56.

Fawcett, D. W., and N. S. McNutt. 1969. The ultrastructure of the cat myocardium. I. Ventricular papillary muscle. *J. Cell Biol.* 42:1–45.

Felder, E., and C. Franzini-Armstrong. 2002. Type-3 ryanodine receptors of skeletal muscle are segregated in a parajunctional position. *Proc. Natl. Acad. Sci. USA.* 99:1695–1700.

Felder, E., F. Protasi, R. Hirsch, C. Franzini-Armstrong, and P. D. Allen. 2002. SR-surface membrane docking in the absence of dihydropyridine receptors and ryanodine receptors. *Biophys. J.* 82:3144–3149.

Ferguson, D. G., and C. Franzini-Armstrong. 1988. The Ca ATPase content of slow and fast twitch fibers of guinea pig. *Muscle Nerve.* 11:561–570.

Flucher, B. E., N. Kasielke, and M. Grabner. 2000. The triad targeting signal of the skeletal muscle calcium channel is localized in the COOH terminus of the α(1S) subunit. *J. Cell Biol.* 151:467–478.

Franzini-Armstrong, C., and D. G. Ferguson. 1985. Density and disposition of CaATPase in sarcoplasmic reticulum membrane as determined by shadowing techniques. *Biophys. J.* 48:607–615.

Franzini-Armstrong, C., and F. Protasi. 1997. The ryanodine receptor of striated muscles—a complex capable of multiple interactions. *Physiol. Rev.* 77:699–729.

Gao, T., M. Bunemann, B. L. Gerhardstein, H. Ma, and M. M. Hosey. 2000. Role of the C-terminus of the α_{1C} ($Ca_V1.2$) subunit in membrane targeting of cardiac L-type calcium channels. *J. Biol. Chem.* 275:25436–25444.

Gilly, W. F., and T. Scheuer. 1984. Contractile activation in scorpion striated muscle fibers. Dependence on voltage and external calcium. *J. Gen. Physiol.* 84:321–345.

Hartzell, H. C., and M. A. Simmons. 1987. Comparison of effects of acetylcholine on calcium and potassium currents in frog atrium and ventricle. *J. Physiol.* 389:411–422.

Inesi, G., R. Wade, and T. Rogers. 1998. The sarcoplasmic reticulum Ca^{2+} pump: inhibition by thapsigargin and enhancement by adenovirus-mediated gene transfer. *Anns. NY. Acad. Sci.* 853:195–206.

Jewett, P. H., J. R. Sommer, and E. A. Johnson. 1971. Cardiac muscle. Its ultrastructure in the finch and hummingbird with special reference to the sarcoplasmic reticulum. *J. Cell Biol.* 49:50–65.

Jones, L. R., Y. J. Suzuki, W. Wang, Y. M. Kobayashi, V. Ramesh, C. Franzini-Armstrong, L. Cleemann, and M. Morad. 1998. Regulation of Ca^{2+} signaling in transgenic mouse cardiac myocytes overexpressing calsequestrin. *J. Clin. Invest.* 101:1385–1393.

Jorgensen, A., A. C.-Y. Shen, W. Arnold, P. S. McPherson, and K. P. Campbell. 1993. The Ca^{2+} release channel/ryanodine receptor s are localized in junctional and corbular sarcoplasmic reticulum in cardiac muscle. *J. Cell Biol.* 120:69–80.

Jorgensen, A. O., A. C. Shen, and K. P. Campbell. 1985. Ultrastructural localization of calsequestrin in adult rat atrial and ventricular muscle cells. *J. Cell Biol.* 101:257–268.

Junker, J., J. R. Sommer, M. Sar, and G. Meissner. 1994. Extended junctional sarcoplasmic reticulum of avian cardiac muscle contains functional ryanodine receptors. *J. Biol. Chem.* 269:1627–1634.

Kavaler, F. 1974. Electromechanical time course in frog ventricle: manipulation of calcium level during voltage clamp. *J. Mol. Cell. Cardiol.* 6:575–580.

Kijima, Y., and S. Fleischer. 1992. Two types of inositol trisphosphate binding in cardiac microsomes. *Biochem. Biophys. Res. Commun.* 189:728–735.

Kijima, Y., A. Saito, T. L. Jetton, M. A. Magnuson, and S. Fleischer. 1993. Different intracellular localization of inositol 1,4,5-trisphosphate and ryanodine receptors in cardiomyocytes. *J. Biol. Chem.* 268: 3499–3506.

Lederer, W. J., M. B. Cannell, N. M. Cohen, and J. R. Berlin. 1989. Excitation-contraction coupling in heart muscle. *Mol. Cell. Biochem.* 89:115–119.

Lipp, P., M. Laine, S. C. Towey, K. M. Burrell, M. J. Berridge, L. Wenhang, and M. D. Bootman. 2000. Functional InsP3 receptors that modulate excitation-contraction coupling in the heart. *Curr. Biol.* 10:939–942.

Mackenzie, L., M. D. Bootman, M. J. Berridge, and P. Lipp. 2001. Predetermined recruitment of calcium release sites underlies excitation-contraction coupling in rat atrial myocytes. *J. Physiol.* 530:417–429.

MacLeod, A. G., A. C.-Y. Shen, K. P. Campbell, M. Michalak, and A. O. Jorgensen. 1991. Frog cardiac calsequestrin: identification, characterization, and subcellular distribution in two structurally distinct regions of peripheral sarcoplasmic reticulum in frog myocardium. *Circ. Res.* 69:344–359.

Meissner, G. 1994. Ryanodine receptor/Ca^{2+} release channels and their regulation by endogenous effectors. *Annu. Rev. Physiol.* 56:485–508.

Morad, M., and L. Cleemann. 1987. Role of Ca^{2+} channel in development of tension in heart muscle. *J. Mol. Cell. Cardiol.* 19:527–553.

Niedergerke, R., D. C. Ogden, and S. Page. 1976. Contractile activation and calcium movements in heart cells. *Symp. Soc. Exp. Biol.* 30:381–395.

Niedergerke, R., and S. Page. 1981a. Analysis of caffeine action in single trabeculae of the frog heart. *Proc. R. Soc.(Lond.) B. Biol. Sci.* 213:303–324.

Niedergerke, R., and S. Page. 1981b. Two physiological agents that appear to facilitate calcium discharge from the sarcoplasmic reticulum in frog heart cells: adrenaline and ATP. *Proc. R. Soc. Lond.* B213:325–344.

Nunzi, M. G., and C. Franzini-Armstrong. 1981. The structure of smooth and striated portions of the adductor muscle of the valves in a scallop. *J. Ultrastructure Res.* 76:134–148.

Ogawa, Y. 1994. Role of ryanodine receptors. *Crit. Rev. Biochem. Mol. Biol.* 29:229–274.

Ojima, K., Z. X. Lin, Z. Q. Zhang, T. Hijikata, S. Holtzer, S. Labeit, H. L. Sweeney, and H. Holtzer. 1999. Initiation and maturation of I-Z-I bodies in the growth tips of transfected myotubes. *J. Cell Sci.* 112:4101–4112.

Olivares, E. B., S. J. Tanksley, J. A. Airey, C. F. Beck, Y. Ouyang, T. J. Deerinck, M. H. Ellisman, and J. L. Sutko. 1991. Non mammalian vertebrate skeletal muscles express two triad junctional foot protein isoforms. *Biophys. J.* 59:1153–1163.

Page, S. 1968. Structure of the sarcoplasmic reticulum in vertebrate muscle. *Br. Med. Bull.* 24:170–173.

Page, S. G., and R. Niedergerke. 1972. Structures of physiological interest in the frog heart ventricle. *J. Cell Sci.* 11:179–203.

Pessah, I. N., R. A. Stambuk, and J. E. Casida. 1987. Ca^{2+}-activated ryanodine binding: mechanisms of sensitivity and intensity modulation by Mg^{2+}, caffeine, and adenine nucleotides. *Mol. Pharmacol.* 31:232–238.

Protasi, F., C. Franzini-Armstrong, and P. D. Allen. 1998. Role of ryanodine receptors in the assembly of calcium release units in skeletal muscle. *J. Cell Biol.* 140:831–842.

Protasi, F., X.-H. Sun, and C. Franzini-Armstrong. 1996. Formation and maturation of the calcium release apparatus in developing and adult avian myocardium. *Dev. Biol.* 173:265–278.

Reuter, H. 1974. Exchange of calcium ions in the mammalian myocardium: mechanism and physiological significance. *Circ. Res.* 34:599–605.

Rousseau, E., and G. Meissner. 1989. Single cardiac sarcoplasmic reticulum Ca^{2+} release channel: activation by caffeine. *Am. J. Physiol.* 256:H328–H333.

Sato, T. 1968. A modified method for lead staining of thin sections. *J. Electron Microscopy.* 17:158–159.

Sommer, J. R. 1995. Comparative anatomy: in praise of a powerful approach to elucidate mechanisms translating cardiac excitation into purposeful contraction. *J. Mol. Cell. Cardiol.* 27:19–35.

Sommer, J. R., E. Bossen, H. Dalen, P. Dolber, T. High, P. Jewett, E. A. Johnson, J. Junker, S. Leonard, R. Nassar, B. Scherer, M. Spach, T. Spray, I. Taylor, N. R. Wallace, and R. Waugh. 1991. To excite a heart: a bird's view. *Acta Physiol. Scand.* 159:5–21. Review.

Sommer, J. R., and E. A. Johnson. 1980. Ultrastructure of cardiac muscle. *In* Handbook of Physiology: The Cardiovascular System, Vol 1. R. Burne, editor. Williams and Wilkins, Baltimore, Maryland. 113–186.

Stern, M. D., and E. G. Lakatta. 1992. Excitation-contraction coupling in the heart: the state of the question. *FASEB J.* 6:3092–3100.

Sun, X.-H., F. Protasi, M. Takahashi, H. Takeshima, D. G. Ferguson, and C. Franzini-Armstrong. 1995. Molecular architecture of membranes involved in excitation-contraction coupling of cardiac muscle. *J. Cell Biol.* 129:659–673.

Sutko, J. L., and J. A. Airey. 1997. Ryanodine receptor Ca^{2+} release channel: does diversity in form equal diversity in function? *Physiol. Rev.* 76:1027–1071.

Takei, K., H. Stukenbrok, A. Metcalf, G. A. Mignery, T. C. Sudhof, P. Volpe, and P. De Camilli. 1992. Ca^{2+} stores in Purkinje neurons: endoplasmic reticulum subcompartments demonstrated by the heterogeneous distribution of the InsP3 receptor, Ca(2+)-ATPase, and calsequestrin. *J. Neurosci.* 12:489–505.

Takekura, H., L. Bennett, T. Tanabe, K. G. Beam, and C. Franzini-Armstrong. 1994. Restoration of junctional tetrads in dysgenic myotubes by dihydropyridine receptor cDNA. *Biophys. J.* 67:793–804.

Takekura, H., B. Flucher, and C. Franzini-Armstrong. 2001. Sequential docking, molecular differentiation and positioning of T-tubule/SR junctions in developing mouse skeletal muscle. *Dev. Biol.* 239:204–214.

Takekura, H., and C. Franzini-Armstrong. 1999. Correct targeting of dihydropyridine receptors and triadin in dyspedic mouse skeletal muscle in vivo. *Dev. Dyn.* 214:372–380.

Takekura, H., M. Nishi, T. Noda, H. Takeshima, and C. Franzini-Armstrong. 1995. Abnormal junctions between surface membrane and sarcoplasmic reticulum in skeletal muscle with a mutation targeted to the ryanodine receptor. *Proc. Natl. Acad. Sci. USA.* 92:3381–3385.

Trafford, A. W., M. E. Diaz, S. C. O'Neill, and D. A. Eisner. 2002. Integrative analysis of calcium signaling in cardiac muscle. *Frontiers Biosci.* 7:843–852.

Tunstall, J., and R. A. Chapman. 1994. The effect of ryanodine on the contraction of isolated frog atrial trabeculae is triggered by caffeine. *Exp. Physiol.* 79:435–444.

Wendt, I. R., and D. G. Stephenson. 1983. Effects of caffeine on Ca-activated force production in skinned cardiac and skeletal muscle fibres of the rat. *Pflugers Arch.* 398:210–216.

Wojcikiewicz, R. J., T. Furuichi, S. Nakade, K. Mikoshiba, and S. R. Nahorski. 1994. Muscarinic receptor activation down-regulates the type I inositol 1,4,5-trisphosphate receptor by accelerating its degradation. *J. Biol. Chem.* 269:7963–7969.